論文 / 著書情報
Article / Book Information

Title	Pressure Induced Variations in Refractive Index of Aromatic Polyimide Film Analyzed by Brillouin Scattering
Authors	Eisuke FUJIWARA, Ryohei ISHIGE, Shota OWAKI, Naohiro KITA, Kenta YAMADA, Takahiro MATSUOKA, Shigeo SASAKI, Shinji ANDO
Citation	Journal of Photopolymer Science and Technology, Vol. 31, No. 5, p. 599-606
Pub. date	2018, 6

Journal of Photopolymer Science and Technology
Volume 31, Number 5 (2018) 607-612 ©2018CPST

Pressure Induced Variations in Refractive Index of Aromatic Polyimide Film Analyzed by Brillouin Scattering

Eisuke Fujiwara[1], Ryohei Ishige[1], Shota Owaki[2], Naohiro Kita[2], Kenta Yamada[2], Takahiro Matsuoka[3], Shigeo Sasaki[3*], and Shinji Ando[1*]

[1] *Department of Chemical Science and Engineering, Tokyo Institute of Technology, Ookayama 2-12-1-E4-5, Meguro-ku, Tokyo 152-8552, Japan*

[2] *Department of Materials Science and Technology, Gifu University, Yanagido 1-1, Gifu 501-1193, Japan*

[3] *Department of Electrical, Electronic and Computer Engineering, Gifu University, Yanagido 1-1, Gifu 501-1193, Japan*
**sando@polymer.titech.ac.jp, ssasaki@gifu-u.ac.jp*

Pressure-induced variations in refractive indices and acoustic velocities of a spin-coated aromatic polyimide (PI) film, poly(4,4'-oxidiphenylene pyromellitimide), were analyzed between atmospheric pressure (0.1 MPa) and 2 GPa by Brillouin scattering measurements with the symmetric platelet and the back scattering geometries for the film surface and the cross-sectional surface. At high pressures, anisotropies in acoustic velocity and refractive indices were clearly observed between the in-plane and out-of-plane directions. Additionally, the average refractive index of the PI film was estimated to increase from 1.682 to 1.80 by applying pressure up to 2 GPa due to the densification of aggregation structures of the PI film.

Keywords: Polyimide, Brillouin Scattering, High Pressure, Refractive Index

1. Introduction

Fully aromatic polyimides (PIs) are high performance engineering plastics exhibiting excellent thermal and chemical stability, radiation resistance, mechanical strength, and flexibility. They have been applied in a wide range of high-tech industries such as aerospace, electric, electronic, and optical applications [1, 2].

Recently, high refractive index PIs have been developed as advanced optical materials by introducing sulfur or selenium atoms in the main chains of PIs [3-13]. The optical properties of PIs also depend strongly on their molecular packing (aggregation) structures. For stimulating and perturbing the aggregation structures of polymer chains in the solid state, application of high pressure is an effective way because it can directly reduce the intermolecular free volume included in polymer solids. The effects of pressurization on the aggregation structures, optical, and physical properties of PIs have been widely investigated by spectroscopic techniques and X-ray scattering methods under high pressure [14-19]. Recently, we have reported the relationship between the optical properties and the aggregation structures of PI films by UV/vis/IR absorption, fluorescence spectra, and synchrotron WAXD patterns measurement under high pressure up to 8 GPa [15-19]. In addition, Chao et al. have examined the pressure-induced variations in acoustic velocity, elastic properties, and density of poly(*p*-phenylene biphenyltetracarboxydiimide) (*s*BPDA/PPD) PI film by using Brillouin scattering method [20]. Furthermore, it has been reported that refractive indices of polymers can be significantly increased by applying pressure due to the increase in density [21-22]. Therefore, we focused on the quantitative measurement of enhanced refractive indices of PI films caused by applying high pressure.

Received March 28, 2018
Accepted May 17, 2018

Since the main chains of PIs consisting of rigid molecular structures are preferentially oriented in the film plane, it is important to consider the anisotropy in physical properties between the in-plane and out-of-plane directions in PI film. In particular, anisotropy in refractive index, *i.e.* in-plane/out-of-plane birefringence, has been widely investigated at atmospheric pressure (0.1 MPa) [23-31], although optical anisotropy of polymer films under high pressure is still hardly investigated by conventional methods.

In this study, the pressure-induced variations in refractive index and acoustic anisotropy of a spin-coated PI film of poly(4,4'-oxidiphenylene pyromellitimide, PMDA-ODA) were investigated by variable pressure Brillouin scattering measurement from 0.1 MPa to 2 GPa by using a diamond anvil cell (DAC).

2. Experimental

2.1. Materials

Pyromellitic dianhydride (PMDA) purchased from Kanto Chemical Co. (Tokyo, Japan) was dried and purified by sublimation under reduced pressure. 4,4'-Diaminodiphenylether (ODA) purchased from Wako Pure Chemical Industries, Ltd. (Osaka, Japan) was purified by recrystallization from tetrahydrofuran (THF), followed by sublimation under reduced pressure. *N*,*N*-dimethylacetamide (anhydrous, 99.8%, DMAc), purchased from Sigma-Aldrich Japan (Tokyo, Japan), was used as received.

2.2. Preparation of PI films

PI films were prepared by conventional two step method by thermal curing of poly(amic acid) (PAA) precursor. The chemical structure of PMDA/ODA is shown in Fig. 1. The PAA solution was prepared by mixing equimolar amounts of dianhydride and diamine in DMAc under dry nitrogen and stirring at room temperature for 48 h. The viscous solution thus obtained was spin-coated on a Si substrate, dried at 70°C for 1 h under N_2, gradually heated to 350°C at 4.6°C min^{-1}, and kept at 350°C for 1.5 h under N_2 to form a PI film. The thickness of the film was ca. 48 μm.

2.3. Refractive index measurement

Since the PI main chains in spin-coated film generally display isotropic orientation in the film plane, anisotropy in refractive index is expressed by a difference between in-plane ($n_{//}$) and out-of-plane ($n_{\perp}$) refractive indices. The $n_{//}$ and $n_{\perp}$ of a PI film at ambient pressure (0.1 MPa) and temperature (22°C) were measured by a Metricon PC-2010 prism coupler at a wavelength (λ) of 636 nm. The average refractive index (n_{av}) was calculated by assuming uniaxial (cylindrical) symmetry; $n_{av}^2 = (2n_{//}^2 + n_{\perp}^2)/3$, and the in-plane/out-of-plane birefringence (Δn) was estimated as $\Delta n = n_{//} - n_{\perp}$. The film thickness was measured by using a sensing-pin-type surface profilometer (Dektak-III, Ulvac, Japan).

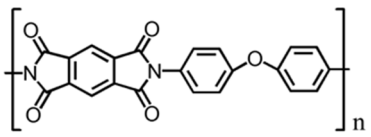

Fig. 1. Molecular structure of PMDA/ODA PI.

2.4. Measurements under high pressure

Variable pressure Brillouin scattering measurements were conducted by using high-pressure DAC in consideration of the anisotropic physical properties in solids [32-36]. The culet size of diamond anvils was about 0.5 mm in diameter, and a hole of stainless steel gasket served as a sample camber of DAC was ca.0.20 mm in diameter and 0.10 mm or less in thickness. A mixture of three types of silicone oils (KF-96-500CS, KF-50-300CS and KF-50-1000CS, Shin-Etsu Co., Ltd., Japan) in a weight ratio of 2:1:1 was used as non-polar pressure transmitting medium. To evaluate the pressure inside the sample chamber, the ruby fluorescence technique was used [37]. Brillouin scattering spectra of a PI film loaded in a DAC at elevated pressures were measured with a 3+3 pass tandem Fabry-Perot interferometer developed by Sandercock [38, 39]. In addition, the Brillouin scattering spectra of the pressure medium without sample film were also measured at elevated pressure in order to separate the Brillouin scattering signals from PI film and pressure medium. Single-frequency continuous green laser ($\lambda_0 = 532$ nm) was used as the Brillouin excitation source and the input power was about 100 W. The laser apparatus is a diode-pumped frequency-doubled solid-state Nd:YVO_4 laser (Showa Optronics Co., Ltd., Japan).

3. Theory and measurement setup

In the Brillouin scattering phenomenon, the momentum conservation law is described as

$$h\boldsymbol{k}_i = h\boldsymbol{k}_s \pm h\boldsymbol{q}, \qquad (1)$$

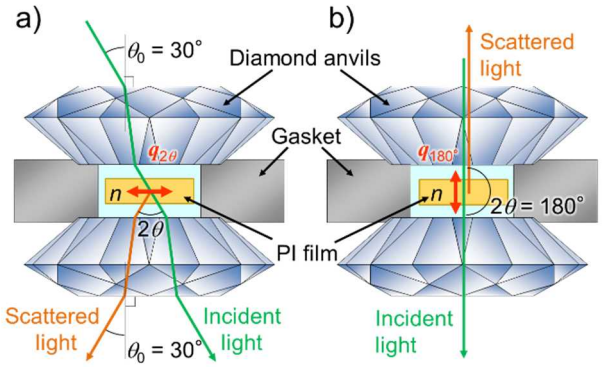

Fig. 2. a) Symmetric platelet Brillouin scattering and b) back Brillouin scattering geometries with a diamond anvil cell. In each geometry, the wave vectors of acoustic phonons are represented as $\boldsymbol{q}_{2\theta}$ and $\boldsymbol{q}_{180°}$.

where $\boldsymbol{q}$ is the wave vector of the acoustic phonon, $\boldsymbol{k_i}$ and $\boldsymbol{k_s}$ are the wave vectors of incident and scattered lights, and h is the Planck constant, respectively. In addition, the energy conservation law is described as

$$h\nu_i = h\nu_s \pm h\Delta\nu, \tag{2}$$

where $\Delta\nu$ is the Brillouin frequency shift, and ν_i and ν_s are the frequencies of incident and scattered lights, respectively. Here, the relations of $\nu_i = c|\boldsymbol{k}_i| = cn/\lambda_0$, $\nu_s = c|\boldsymbol{k}_s|$ and $\Delta\nu = V|\boldsymbol{q}|$ hold, where c is the velocity of light, V is the acoustic velocity, n is the refractive index along the polarization direction of incident light in the PI film, and λ_0 is the wavelength of the incident light for excitation in vacuum. Since the relation of $|\boldsymbol{q}| = 2n\sin\theta/\lambda_0$ holds due to $c >> V$, the Brillouin frequency shift $\Delta\nu$ can be expressed as

$$\Delta\nu = V|\boldsymbol{q}| = \frac{2nV\sin\theta}{\lambda_0}, \tag{3}$$

where θ is the half of scattering angle [40].

As shown in Fig. 2, Brillouin scattering measurements were conducted in a symmetric platelet scattering geometry ($2\theta_0$ = 60°) using s-polarized incident light and a back (180°) scattering geometry for direct determination of the V and n. In the symmetric platelet scattering geometry, the incident angle at the interface between air and diamond anvil was set at 30° and the scattered light with output angle of 30° in air was detected from the opposite side of the pair of anvil planes. In the back scattering geometry, the incident angle was set at 0° (normal incident) and the scattered light propagating backward (output angle of 180°) was detected.

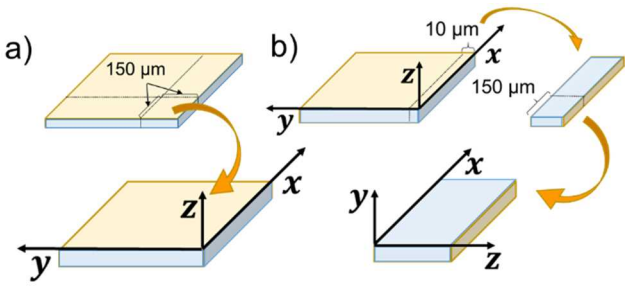

Fig. 3. Schematic drawing of procedures for preparation of a) Surface sample and b) Cross-section sample.

In the symmetric platelet scattering, the scattering angle 2θ is expressed as $2\cdot\sin^{-1}(1/2n)$ [$= 2\sin^{-1}(\sin\theta_0/n)$]. Hence, the eq. (3) can be simplified to

$$\Delta\nu_{60} = \frac{V_{\parallel}}{\lambda_0}, \tag{4}$$

where the direction of acoustic velocity $V_{\parallel}$ is parallel to the anvil plane. On the other hand, the eq. (3) for back scattering can be simplified to

$$\Delta\nu_{180} = \frac{2nV_{\perp}}{\lambda_0}, \tag{5}$$

where the direction of acoustic velocity $V_{\perp}$ is perpendicular to the anvil plane, and the n is the refractive index along the polarization direction of the incident light. By combining eqs. (4) and (5), the following equation can be obtained when we can assume $V_{\parallel} = V_{\perp}$.

$$n = \frac{\Delta\nu_{180}}{2\Delta\nu_{60}} \tag{6}$$

For a spin-coated PI film having optical anisotropy, in-plane/out-of-plane birefringence (Δn) is to be considered, and two kinds of measurements from different film planes; surface plane and cross-sectional plane, are required to evaluate the anisotropy in refractive index. Two surface planes were prepared by different cutting methods as shown in Fig. 3. For the surface plane measurement, a sample was prepared by cutting a PI film directly into a square of 150 μm on one side (hereafter called 'Surface sample') (Fig. 3 a). For the cross-sectional plane, another sample was prepared by the following procedure. Firstly, a PI film was cut into a stripe with a width of 10 μm, which is smaller than the film thickness (48 μm), and then the stripe was cut by 150 μm interval to form cross-sectional surfaces (called 'Cross-section sample') (Fig. 3b)). For each sample, the coordinate system was set as

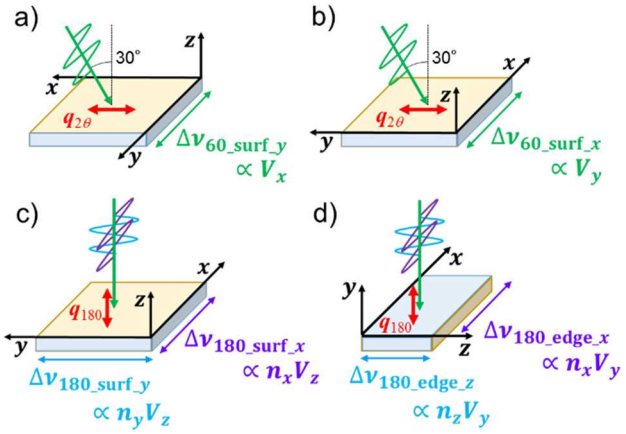

Fig. 4. Schematic illustrations of Brillouin scattering geometries for symmetric platelet scattering of the Surface sample by incident lights polarized in the direction of a) *y*- or b) *x*-axis, and for back scattering of c) Surface and d) Cross-section (edge) sample.

shown in Fig. 3.

The schematic illustrations for the geometries of Brillouin scattering measurement are shown in Fig. 4. For the Surface sample, the symmetric platelet and the back Brillouin scattering measurements were conducted (Figs. 4 a,b,c). In the symmetric platelet geometry, *s*-polarized incident light was used to evaluate V_x and V_y, respectively. In the back-scattering geometry, incident light polarized in the direction of *x*- or *y*-axis was used to evaluate the values of n_xV_z and n_yV_z. For the Cross-section (edge) sample, the back Brillouin scattering measurement was performed (Fig. 4 d). The polarization direction of the incident light was adjusted to the *x*- or *z*-axis. The sample plane and polarization direction of the incident light are shown as a subscript of Brillouin frequency shift. For example, $\Delta\nu_{60\_surf\_x}$ represents the symmetric platelet scattering Brillouin frequency shift measured form the surface plane with the incident light polarized along the *x*-axis. The propagating direction of acoustic velocity and the polarizing direction for refractive index are shown as a subscript, e.g. V_x and n_x.

4. Results and discussion

4.1. Refractive index of PI film

The $n_{//}$ and $n_{\perp}$ of a PI film were measured at 636 nm as 1.7018 and 1.6430 by a prism coupler, and the n_{av} and Δn were calculated as 1.6824 and 0.0589, respectively. The positive Δn value indicates that PI main chains are preferentially orientated in the in-plain direction. Due to the large thickness (48 μm), the Δn value was relatively smaller than those of thinner films having the same chemical structure (Δn = 0.0841 for a 9 μm-thick and Δn = 0.0693 for a 12−15 μm-thick film) [30, 31].

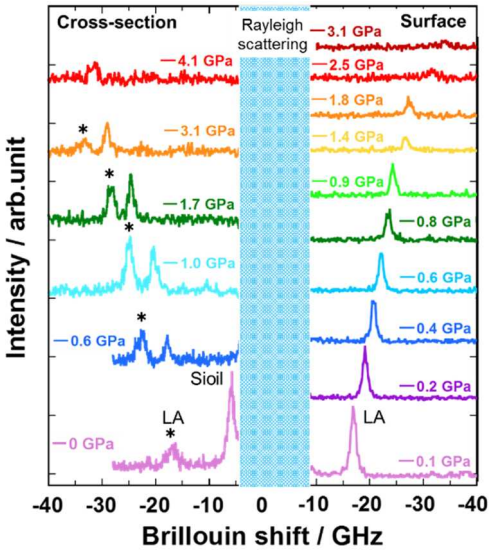

Fig. 5. Brillouin scattering spectra of Surface (right side) and Cross-section (left side) sample at each pressure measured by back scattering geometry with the incident light polarized along *x*-axis. Strong Rayleigh scattering is shaded at around 0 GHz.

4.2. Pressure-induced variations in Brillouin frequency shifts of PI film

The pressure-induced variations in the in-plane/out-of-plane refractive indices and acoustic velocities of the PI film were investigated at elevated pressures from 0.1 MPa to 2 GPa for the surface and cross-section planes by Brillouin scattering measurements. Brillouin scattering spectra of the surface and cross-section planes at each pressure are presented in Fig. 5. These spectra were measured in the back scattering geometry with an incident light polarized along the *x*-axis. For the Cross-section sample, two peaks were observed, in which the peaks at larger frequencies of the Brillouin shift, marked by asterisks, are attributable to the longitudinal acoustic (LA) mode of the PI film. The peak appearing at the smaller shift at each pressure is originated from the pressure medium. On the other hand, all the peaks observed for the Surface sample at elevated pressures are attributable to the LA mode of the PI film. The LA peaks show gradual increases in their Brillouin frequency shifts with increasing the pressure, although the peak from the PI film completely disappeared at 4.1 GPa. This is because the incident laser light (λ = 532 nm) was strongly absorbed by the PI film due to the bathochromic shifts of the absorption edge caused by enhancement of the intermolecular charge transfer (CT) interactions. The enhanced absorbance of the PI film at 532 nm significantly reduced the light scattering of incident light [9, 11].

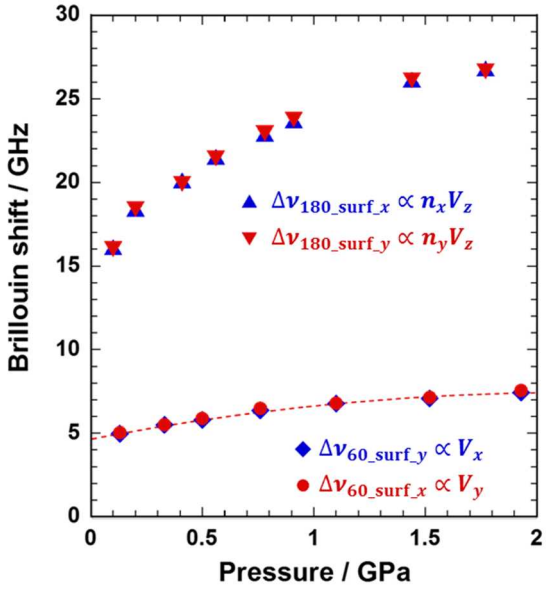

Fig. 6. Pressure-induced variations in Brillouin frequency shifts of the Surface sample at symmetric platelet and back Brillouin scattering geometries. (The dashed line is described as eq. 12.)

Fig. 6 presents the pressure-induced variations in Brillouin frequency shifts in the surface plane (Surface sample) measured with the symmetric platelet and the back Brillouin scattering geometries. Firstly, the acoustic and optical properties in the *xy*-plane were evaluated by the two geometries for Surface sample (Fig. 4 a,b,c). The values of $\Delta\nu_{60\_surf\_y}$ and $\Delta\nu_{60\_surf\_x}$, which are proportional to the V_x and V_y respectively (eq. 4), at each pressure are similar to each other, which indicates that no specific acoustic anisotropy exists in the *xy*-plane. In addition, there are no differences between the values of $\Delta\nu_{180\_surf\_x}$ and $\Delta\nu_{180\_surf\_y}$, which are proportional to the n_xV_z and n_yV_z respectively (eq. 5), at each pressure. Thereby, we can conclude that the anisotropy in acoustic velocity and refractive index in the *xy*-plane is negligibly small in the pressure range between 0.1 MPa and 2 GPa.

Secondly, the acoustic and optical properties in the *xz*-plane were investigated based on the back Brillouin scattering measurements of the two samples (Fig. 4 c,d). The pressure-induced variations in $\Delta\nu_{180\_surf\_x}$ and $\Delta\nu_{180\_edge\_x}$ can be compared in Fig. 7. The dashed lines were obtained by the least-squares second-order polynomial fitting to the plots of the Cross-section sample. These fitted lines can be expressed as follows.

$$\Delta\nu_{180\_surf\_x} = -3.33\,P^2 + 12.2\,P + 15.5 \qquad (7)$$

$$\Delta\nu_{180\_edge\_x} = -2.06\,P^2 + 9.96\,P + 17.2, \qquad (8)$$

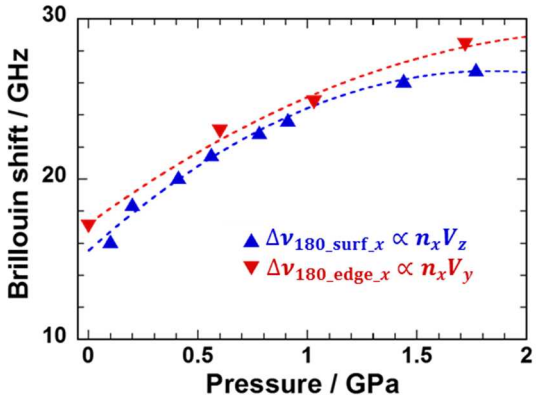

Fig. 7. Pressure-induced variations in Brillouin frequency shifts of the Surface and Cross-section sample at back Brillouin scattering geometries. (The dashed lines are described as eq. 7 and 8.)

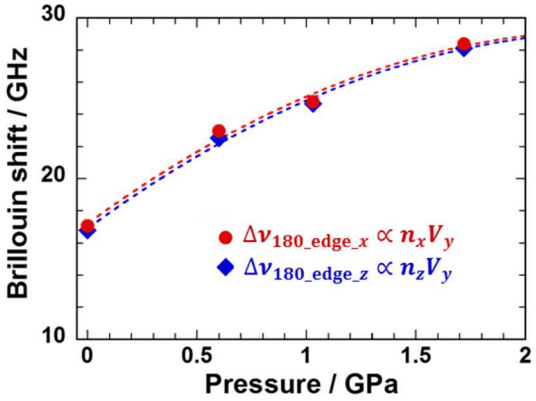

Fig. 8. Pressure-induced variations in Brillouin frequency shifts of the Cross-section sample at back Brillouin scattering geometries. (The dashed lines are described as eqs. 8 and 11.)

where P is pressure in GPa. As shown in Fig. 7, the values of $\Delta\nu_{180\_edge\_x}$ are obviously larger than those of $\Delta\nu_{180\_surf\_x}$, and the differences between $\Delta\nu_{180\_edge\_x}$ and $\Delta\nu_{180\_surf\_x}$ were 2.78−10.7 % in the pressure range between 0.1 MPa to 2 GPa. Since the $\Delta\nu_{180\_surf\_x}$ and $\Delta\nu_{180\_edge\_x}$ values are proportional to the n_xV_z and n_xV_y values, respectively, the difference between these lines corresponds to the anisotropy between V_y (= $V_{//}$) and V_z (= $V_\perp$). Gomopoulos et al. [41] reported that the acoustic anisotropy for a 10−20 μm-thick spin-coated film of *s*BPDA/PPD PI. The PI film exhibited the much larger in-plane acoustic velocity $V_{//}$ (3,560 m/s) than the out-of-plane acoustic velocity $V_\perp$ (2,340 m/s) as well as the $n_{//}$ and $n_\perp$ values as 1.893 and 1.663, respectively at 532 nm. Thus, the positive acoustic anisotropy ($V_{//} > V_\perp$) at each pressure shown in Fig. 7 indicates that the PI film exhibited the positive optical anisotropy ($n_{//} > n_\perp$) which should be caused by the in-plane orientation of the PI main chains. Moreover, the acoustic anisotropy, which is defined as $\eta = (V_{//} - V_\perp)/(2V_{//}+V_\perp)$, of the PMDA-ODA PI film can be

estimated as 0.0274 at 0.1 MPa based on eq. 7 and 8, which is much smaller than the value of *s*BPDA/PPD film (η = 0.129) [41]. The in-plane /out-of-plane birefringence of the former film at 0.1 MPa measured by the prism coupling method (Δn = 0.0589) is also much smaller than the value of the latter film (Δn = 0.230). Thereby, both the large acoustic and optical anisotropies observed for the *s*BPDA/PPD were originated from its significant in-plane orientation of the PI main chains.

4.3. Pressure-induced variations in refractive indices of PI film

The pressure dependence of optical properties in the xz-plane is discussed based on $\Delta\nu_{180\_edge\_x}$ and $\Delta\nu_{180\_edge\_z}$ as plotted in Fig. 8. The values of $\Delta\nu_{180\_edge\_x}$ and $\Delta\nu_{180\_edge\_z}$ are proportional to those of n_xV_y and n_zV_y values, respectively. Hence, the pressure-induced variations in n_x and n_z can be estimated based on eq. (6) by dividing $\Delta\nu_{180\_edge\_x}$ ($\propto n_xV_y$) (eq. 8) and $\Delta\nu_{180\_edge\_z}$ ($\propto n_zV_y$) by $\Delta\nu_{60\_surf\_x}$ ($\propto V_y$), respectively, as

$$n_x(P) = \frac{\Delta\nu_{180\_edge\_x}}{2\Delta\nu_{60\_surf\_x}} \quad (9)$$

$$n_z(P) = \frac{\Delta\nu_{180\_edge\_z}}{2\Delta\nu_{60\_surf\_x}} \quad (10)$$

The pressure-induced variations in $\Delta\nu_{180\_edge\_z}$ and $\Delta\nu_{60\_surf\_x}$ were obtained by the least-squares second-order polynomial fitting to the plots of Brillouin shifts in Figs. 8 and 6, respectively as follows.

$$\Delta\nu_{180\_edge\_z} = -2.04\,P^2 + 10.0\,P + 16.9, \quad (11)$$

$$\Delta\nu_{60\_surf\_x} = -0.586\,P^2 + 2.55\,P + 4.75. \quad (12)$$

Figure 9 presents the pressure dependence of in-plane and out-of-plane refractive indices, $n_x(P)$ and $n_z(P)$, estimated for the *xz*-plane of the PI film by Brillouin scattering. Note that the values of $n_x(P)$ are larger than those of $n_z(P)$ at each pressure. The observed positive optical anisotropy ($n_x > n_z$) in the PI film accords well with that from the prism coupling ($n_{//} > n_{\perp}$) as well as the positive in-plane/out-of-plane anisotropy in acoustic velocity ($V_x > V_z$). The in-plane/out-of-plane birefringence (Δn) at 0.1 MPa was estimated as 0.0316, which is slightly smaller than that from the prism coupling method (Δn = 0.0589). The relatively small birefringence obtained from Brillouin scattering could be caused by the broadening of scattering peaks in Fig. 5 and a failure of the back-scattering

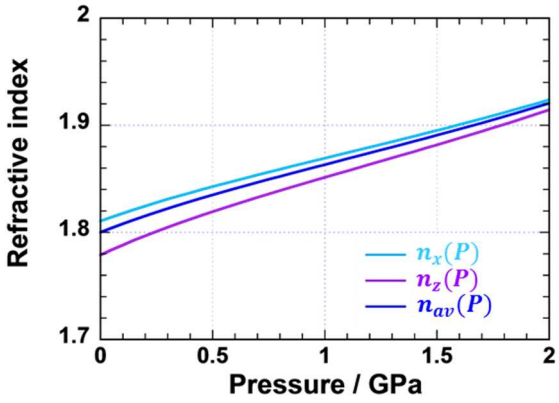

Fig. 9. Pressure-induced variations in n_x, n_z, and average refractive index n_{av}, estimated by Brillouin scattering measurements of the PI film.

condition (2θ = 180°) due to the surface roughness with tooth marks made by a blade on the cross-sectional plane.

In the following part, the pressure dependence of average refractive index n_{av} of the PI film is discussed, in which n_{av} is defined as

$$n_{av}(P) = \sqrt{\frac{2n_x^2(P) + n_z^2(P)}{3}} \quad (13)$$

With increasing the pressure, n_{av} gradually increases from 1.80 at 0.1 MPa to the highest value of 1.92 at 2 GPa as shown in Fig. 9. Note that the n_{av} value at 0.1 MPa is significantly larger than that measured by the prism coupling method (n_{av}=1.682), which could be caused by the following reasons. One is the surface roughness of the cross-sectional plane as stated above, and the other is that the estimated value of $\Delta\nu_{60\_surf\_x}$ ($\propto V_y$) at 0.1 MPa according to eq. 12 was smaller than the true value. Assuming a systematic deviation between the two methods as 0.118 (δn = 1.80 − 1.682), the n_{av} at 2 GPa by prism coupling can be estimated as ca.1.80. To our best knowledge, the highest refractive index of PI films was reported as 1.760−1.768 at 633 nm, and all of them contain plural sulfur atoms in the main chains [3,9,13], in which the weight contents of sulfur atoms were as high as 23.2−30.1 wt%. Hence, the n_{av} value of 1.80 is obviously larger than those of the sulfur containing PIs ever reported. Therefore, we can conclude that the average refractive index of PI film can be significantly enhanced at elevated pressures up to 2 GPa.

According to the Lorentz-Lorenz formula,

$$\frac{n_{av}^2 - 1}{n_{av}^2 + 2} = \left(\frac{4}{3}\pi\right)\left(\frac{\rho}{M}\right)N_A\alpha\ , \quad (14)$$

where M is the molecular weight of the repeating unit, and N_A is the Avogadro's number, the pressure-induced enhancement of refractive index (n_{av}) could be directly related to an increase in density (ρ) of the PI film because the average molecular polarizability of the repeating unit (α) would not be significantly influenced by pressure. A remarkable decrease in inter-chain distances of PI chains induced by high pressure was also detected by wide-angle X-ray diffraction and spectroscopic techniques [18,19]. Hence, this should also directly lead to an increase in the density of PI films, which results in the enhancement of the refractive index under high pressure.

Finally, it should be noted that the enlarged Brillouin shifts observed at elevated pressures were totally recovered to the original value at 0.1 MPa after releasing the pressure. This clearly indicates that the compression behavior of PI film executed in DAC was elastic and reversible. Thereby, novel ideas are required to fix and maintain the highly compressed aggregated states, thus generated at high pressure (~2 GPa), even at atmospheric pressure. An attempt to retain a part of such unique properties and structures by using chemical or thermal crosslinking is under way. We hope that the use of high pressure will become an effective and useful method to enhance the physical properties of functional aromatic polymers applicable to opto-electronics, photonics, and aero-space applications.

5. Conclusion

The pressure dependences of refractive index and anisotropy in acoustic velocity of a 48 μm-thick PMDA/ODA PI film were investigated by variable pressure Brillouin scattering measurements from atmospheric (0.1 MPa) up to 2 GPa. To take into account the optical and acoustic anisotropy, two different geometries were adopted; the incident planes are perpendicular to the film surface or to the cross-section. At each pressure, anisotropies in acoustic velocities and refractive indices were clearly observed between in-plane and out-of-plane directions of the PI film. Additionally, the estimated average refractive index n_{av} of the PI film was increased from 1.682 to 1.80 by 7.0 % due to the densification of aggregation structures of the PI film up to 2 GPa, which indicates that a very high refractive index can be achieved by applying pressure. Consequently, Brillouin scattering measurement is an effective and versatile method to investigate the acoustically and optically anisotropic properties of polymer films subject to high pressure.

Acknowledgement

This work was supported in part by Grants-in-Aid for Scientific Research, Japan Society for the Promotion of Science (25288096 and 15K2099). The authors thank Prof. Kei Hirose and Dr. Shigehiko Tateno at the Department of Earth and Planetary Sciences, Tokyo Institute of Technology, for the advice on diamond anvil cell.

References

1. C. E. Stroog, *J. Polym. Sci.: Macromol. Rev.*, **23** (1976) 161.
2. G. Rabilloud, '*High-Performance Polymers: Polyimides in Electronics*' Technip Editions (Paris, France) (2000).
3. J. G. Liu, Y. Nakamura, Y. Suzuki, Y. Shibasaki, S. Ando, and M. Ueda, *Macromolecules*, **40** (2007) 4614.
4. J. G. Liu, Y. Nakamura, Y. Shibasaki, S. Ando, and M. Ueda, *J. Polym. Sci. Part A: Polym. Chem.*, **45** (2007) 5606.
5. J. G. Liu, Y. Nakamura, Y. Suzuki, Y. Shibasaki, S. Ando, and M. Ueda, *Macromolecules*, **40** (2007) 7902.
6. J. G. Liu, Y. Nakamura, T. Ogura, Y. Shibasaki, S. Ando, and M. Ueda, *Chem. Mater.*, **20** (2008) 273.
7. R. Okutsu, S. Ando, and M. Ueda, *Chem. Mater.*, **20 (**2008) 4017.
8. R. Okutsu, Y. Suzuki, S. Ando, and M. Ueda, *Macromolecules*, **41** (2008) 6165.
9. N. H. You, Y. Suzuki, D. Yorifuji, S. Ando, and M. Ueda, *Macromolecules*, **41** (2008) 6361.
10. C. A. Terraza, J. G. Liu, Y. Nakamura, Y. Shibasaki, S. Ando, and M. Ueda, *J. Polym. Sci. Part A: Polym. Chem.*, **46** (2008) 1510.
11. N. H. You, Y. Suzuki, T. Higashihara, S. Ando, and M. Ueda, *Polymer*, **50** (2009) 789.
12. Y. Suzuki, T. Higashihara S. Ando, and M. Ueda, *Eur. Polym. J.*, **46** (2010) 34.
13. N. Fukuzaki, T. Higashihara, S. Ando, and M. Ueda, *Macromolecules*, **43** (2010) 1836.
14. D. Erskine, P. Y. Yu, and S. C. Freilich, *J. Polym. Sci., Part C*, **26** (1998) 465.
15. K. Takizawa, J. Wakita, M. Kakiage, H. Masunaga, and S. Ando, *Macromolecules*, **43** (2010) 2115.
16. K. Takizawa, H. Fukudome, K. Yukiko, and S. Ando, *Macromolecules*, **47** (2014) 3951.
17. J. Wakita, and S. Ando, *J. Phys. Chem. B*, **113** (2009) 8835.
18. K. Takizawa, J. Wakita, S. Azami, and S. Ando, *Macromolecules*, **44** (2010) 349.
19. K. Takizawa, J. Wakita, K. Sekiguchi, and S.

Ando, *Macromolecules*, **45** (2012) 4764.
20. J. Wang, X. Zhao, B. B. Eril, C. Chen, K. Wang, S. Chen, B. Zou, B. Liu, Q. Zhou, F. Li, and D. Chao, *Polymer*, **90** (2016) 1.
21. M. S. Jeong, J. H. Kim, J. H. Ko, Y. H. Ko, and K. J. Kim, *Curr. Appl. Phys*., **13** (2013) 1774.
22. T. Plisson, P. C. Lalu, G. Huse, and P. Loubeyyre, *J. Appl. Phys.*, **120** (2016) 085903.
23. L. Lin, and S. A. Bidstrup, *J Appl. Polym. Sci.*, **49** (1993) 1277.
24. H. C. Liou, P. S. Ho, and R. Stieman, *Thin Solid Films*, **339** (1999) 68.
25. M. Ree, C. W. Chu, and M. J. Goldberg, *J Appl. Phys.*, **75** (1994) 1410.
26. M. Ree, K. Kim, S. H. Woo, and H. Chung, *J Appl. Phys.*, **81** (1997) 698.
27. K. Nakagawa, *J Appl. Polym. Sci.*, **41** (1990) 2049.
28. S. S. Hardaker, S. Moghazy, C. Y. Cha, and R. J. Samuels, *J Polym. Sci. Part B: Polym. Phys.*, **31** (1993) 1951.
29. S. Ando, T. Sawada, and S. Sasaki, *Polym. Adv. Technol.*, **12** (2000) 319.
30. S. Ando, Y. Watanabe, and T. Matsuura, *Jpn. J. Appl. Phys.*, **41** (2002) 5254.
31. Y. Terui, and S. Ando, *J. Appl. Phys.*, **116** (2014) 053524.
32. H. Shimizu, and S. Sasaki, *Science* **257** (1992) 514.
33. S. Sasaki, and H. Shimizu, *J. Phys. Soc. Jpn.*, **64**, (1995) 3309.
34. H. Shimizu, T. Kitagawa, and S. Sasaki, *Phys. Rev. B*, **47** (1993) 11567.
35. H. Shimizu, N. Nakashima, and S. Sasaki, *Phys. Rev.*, *B* **53** (1996) 111.
36. T. Kume, M. Daimon, S. Sasaki, and H. Shimizu, *Phys. Rev.*, *B* **57** (1998) 13347.
37. G. J. Piermarini, S. Block, and J. D. Barnett, *J. Appl. Phys*., **44** (1973) 5377.
38. J. R. Sandercock, *Opt. Commun.*, **2** (1970) 73.
39. J. R. Sandercock, *Proc. Intn. Conf. Light Scattering in Solids*, Paris, eds. M. Balkanski (Flammarion, Paris) (1971) 9.
40. H. Shimizu, E. M. Brody, H. K. Mao, and P. M. Bell, *Phys. Rev. Lett.* **47** (1981) 128.
41. N. Gomopoulos, G. Saini, M. Efremov, P. F. Nealey, K. Nelson, and G. Fytas, *Macromolecules*, **43** (2010) 1551.